A Non-Linear Model for the Longitudinal Dynamics of a Hypersonic Air-breathing Vehicle

Michael A. Bolender *

David B. Doman †

Air Force Research Laboratory, Wright-Patterson AFB, OH 45433

A non-linear, physics-based model of the longitudinal dynamics for an air-breathing hypersonic vehicle is developed. The model is derived from first principles and captures the complex interactions between the propulsion system, aerodynamics, and structural dynamics. Unlike conventional aircraft, hypersonic vehicles require that the propulsion system be highly integrated into the airframe. Furthermore, hypersonic aircraft tend to have very lightweight, flexible structures that have low natural frequencies. Therefore, the first bending mode of the fuselage is important as its deflection affects the amount of airflow entering the engine, thus influencing the performance of the propulsion system. The equations-of-motion for the flexible aircraft are derived using Lagrange's Equations. The equations-of-motion capture inertial coupling effects between the pitch and normal accelerations of the aircraft and the structural dynamics. The linearized aircraft dynamics are shown to be unstable, and in most cases, exhibit non-minimum phase behavior. The linearized model also indicates that there is an aeroelastic mode that has a natural frequency more than twice the frequency of the fuselage bending mode. Furthermore, the short-period mode is very strongly coupled with the bending mode of the fuselage.

Introduction

Air-breathing hypersonic aircraft are seen as a possible solution to making access to space routine and affordable. Research into air breathing hypersonics began during the 1960's and continued through the 1990's with the National Aerospace Plane. After the cancellation of the National Aerospace Plane in the early 1990's, there have been a handful of follow-on programs that were mostly intended to demonstrate the feasibility of the various technologies needed to achieve sustained hypersonic flight. The most recent example has been NASA's successful flight tests of the scramjet powered X-43A in 2004.

In the literature, there have been several papers that discuss the challenges associated with the dynamics and control of air-breathing hypersonic vehicles (HSVs).[1,2] Air-breathing hypersonic vehicles, similar to that shown in Figure 1, have a tightly integrated airframe and scramjet propulsion system. The configuration in Figure 1 is very typical of an air-breathing hypersonic vehicle. The design is such that the forward fuselage of the aircraft, in conjunction with the bow shock, acts as a compression system for the scramjet propulsion system. The pressure distribution on the forebody also produces lift and a nose-up pitching moment. Downstream of the scramjet engine, the aircraft is shaped such that there is an external expansion of the exhaust gases. The pressure on the aftbody is a function of the pressure of the exhaust gas as it exits the scramjet engine. The expansion of the exhaust gas contributes to the lift of the vehicle, partially offsets the drag, and balances the vehicle with a nose-down pitching moment. With the engine below the center-of-gravity, the thrust produces a nose-up pitching moment that must be balanced by the elevator. The structural modes for this class of vehicle also play an important role. The vibrating, forward fuselage effectively changes the pressure distribution over the forebody of the aircraft since it changes the apparent

*Aerospace Engineer. Senior Member AIAA.

†Senior Aerospace Engineer. Associate Fellow AIAA.

Report Documentation Page

Form Approved
OMB No. 0704-0188

1. REPORT DATE	2. REPORT TYPE	3. DATES COVERED
2006		**00-00-2006 to 00-00-2006**

4. TITLE AND SUBTITLE	5a. CONTRACT NUMBER
A Non-Linear Model for the Longitudinal Dynamics of a Hypersonic Air-breathing Vehicle	5b. GRANT NUMBER
	5c. PROGRAM ELEMENT NUMBER
6. AUTHOR(S)	5d. PROJECT NUMBER
	5e. TASK NUMBER
	5f. WORK UNIT NUMBER
7. PERFORMING ORGANIZATION NAME(S) AND ADDRESS(ES) **Air Force Research Laboratory,Air Vehicles Directorate,Wright Patterson AFB,OH,45433**	8. PERFORMING ORGANIZATION REPORT NUMBER
9. SPONSORING/MONITORING AGENCY NAME(S) AND ADDRESS(ES)	10. SPONSOR/MONITOR'S ACRONYM(S)
	11. SPONSOR/MONITOR'S REPORT NUMBER(S)

12. DISTRIBUTION/AVAILABILITY STATEMENT
Approved for public release; distribution unlimited

13. SUPPLEMENTARY NOTES
The original document contains color images.

14. ABSTRACT

15. SUBJECT TERMS

16. SECURITY CLASSIFICATION OF:			17. LIMITATION OF ABSTRACT	18. NUMBER OF PAGES	19a. NAME OF RESPONSIBLE PERSON
a. REPORT	b. ABSTRACT	c. THIS PAGE			
unclassified	**unclassified**	**unclassified**		**22**	

Figure 1. X-43 Hypersonic Vehicle Concept

turn angle of the flow. The resulting changes in the pressure distribution over the aircraft are realized downstream not only as thrust perturbations, but lift, drag and pitching moment perturbations as well.

In this paper, we present a model that captures the structural, aerodynamic, and propulsion system coupling. The first attempt at a comprehensive analytical model of the longitudinal dynamics of an HSV was undertaken by Chavez and Schmidt.[3] The approach taken here differs from that followed by Chavez and Schmidt.[3] To begin, they assumed the geometry shown in Figure 2. To estimate the aerodynamic forces and moments on the vehicle, Newtonian Impact Theory was employed. The use of Newtonian Impact Theory allowed for a straightforward determination of the expressions for the pressures acting on the vehicle. The pressures were dependent upon vehicle Mach number, freestream pressure, angle-of-attack, and the vehicle geometry. These expressions were then manipulated to give the total aerodynamic forces on the vehicle. The resulting equations were then linearized to give analytical expressions for the stability and control derivatives. Ultimately, requirements and control laws for the Chavez/Schmidt HSV were synthesized.[1,4]

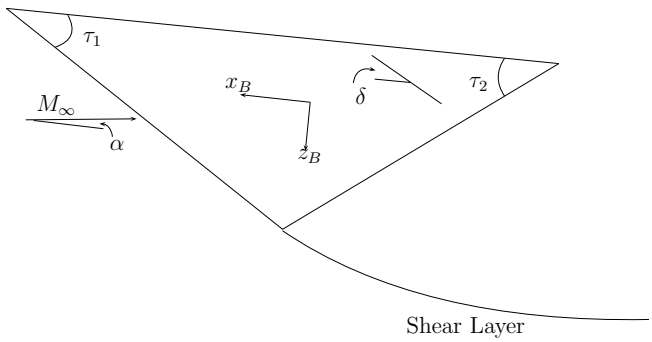

Figure 2. HSV Geometry from Reference 3

The approach of Rudd and Pines[5] was to apply a computational fluid dynamics code written to optimize the design a caret-wing-wedge hypersonic wave rider. The code was then used to study the propulsion/airframe integration and to estimate the stability and control derivatives. These stability and control

derivatives were then compared to those estimated using "hypersonic piston theory." The vehicle design included a translating engine cowl to maintain a shock-on-lip condition. An LQR control design was performed for the stability and control derivatives derived using both approaches. As expected, the piston theory approach was not able to account for the integrated airframe/propulsion system. As a result, the controller designed using the piston theory estimates for the stability and control derivatives was unstable in the non-linear 3DOF simulation that used the stability and control derivatives calculated using the CFD code.

Two models from NASA include the GHAME model from Dryden Flight Research Center, and the NASA Langley model. The latter aircraft is a canard-configured, generic winged-cone configuration that is intended to be representative of a single-stage-to-orbit accelerator type of vehicle. The stability and control derivatives were estimated using a subsonic/supersonic panel code and a hypersonic local surface inclination method. The GHAME model is also a single-stage-to-orbit aircraft.

Aerodynamic and Propulsive Force Determination

The approach that is taken here extends the work done by Chavez and Schmidt.[3] The primary difference being that instead of using Newtonian Impact Theory to calculate the surface pressure, we apply oblique-shock and Prandtl-Meyer theory. Additionally, our vehicle uses a translating cowl door that is used to maintain a shock-on-lip condition for off-design flight conditions. To position the cowl-door necessitates that one is able to determine the angle that the oblique shock makes relative to the freestream. Newtonian Impact Theory assumes that the oblique bow shock lies very close to the body as $M_\infty \to \infty$. In actuality, the angle that the oblique shock makes relative to the freestream is not indicative of its actual angle at the lower end of the hypersonic speed range. Therefore, we are relegated to using oblique-shock theory for our pressure calculation on the lower forebody in order to know the angle of the oblique shock..

The vehicle geometry that was chosen for this work is shown in Figure 3. It is assumed that the vehicle shown has unity depth into the paper and that air behaves as if it is a perfect gas (i.e., $\gamma = c_p/c_v = 1.4$ is a constant).

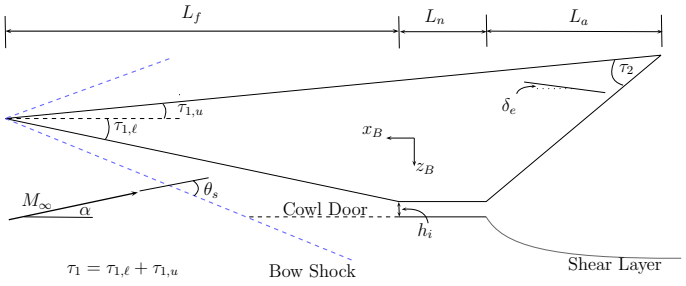

Figure 3. Hypersonic Air-breathing Vehicle Geometry

Forebody and Upper Surface Pressures

The pressure on the forebody is determined by either oblique shock theory or Prandtl-Meyer flow and is dependent upon the angle-of-attack and the amount of structural bending. For angles-of-attack greater than the angle $-\tau_{1\ell}$, the flow behaves as if it is flowing over a concave corner; therefore, an oblique shock occurs ahead of the lower forebody. The shock angle with respect to the horizontal (in this case taken to be the direction of the oncoming freestream flow), is a function of angle-of-attack and $\tau_{1\ell}$. The shock angle is

calculated by solving the following polynomial for $\sin^2\theta_s$

$$\sin^6\theta_s + b\sin^4\theta_s + c\sin^2\theta_s + d = 0 \tag{1a}$$

$$b = -\frac{M_1^2+2}{M_1^2} - \gamma\sin^2\delta \tag{1b}$$

$$c = \frac{2M_1^2+1}{M_1^4} + \left(\frac{(\gamma+1)^2}{4} + \frac{\gamma-1}{M_1^2}\right)\sin^2\delta \tag{1c}$$

$$d = -\frac{\cos^2\delta}{M_1^4} \tag{1d}$$

where M_∞ is the Mach number upstream of the oblique shock, γ is the ratio of specific heats, and $\delta = \tau_{1\ell} + \alpha$ is the angle (in radians) through which the flow is turned. The angle of the oblique shock is given by the second root of Equation (1a) as this particular wave angle corresponds to the weak shock solution. The smallest of the three roots corresponds to a decrease in entropy. Since this solution is not physically realizable, it is discarded. The largest root is the strong shock solution, and is not of interest as the back pressures are not strong enough to support this solution.

Once the shock angle is determined, the pressure, temperature, and Mach number behind the oblique shock can be determined from the relations:[6]

$$\frac{p_2}{p_1} = \frac{7M_1^2\sin^2\theta_s - 1}{6} \tag{2}$$

$$\frac{T_2}{T_1} = \frac{(7M_1^2\sin^2\theta_s - 1)(M_1^2\sin^2\theta_s + 5)}{36M_1^2\sin^2\theta_s} \tag{3}$$

$$M_2^2\sin^2(\theta_s - \delta) = \frac{M_1^2\sin^2\theta_s + 5}{7M_1^2\sin^2\theta_s - 1} \tag{4}$$

where M_1, T_1, p_1 are the Mach number, static temperature, and static pressure upstream of the oblique shock.

On the other hand, in the cases where we have flow over a convex corner, we will have a Prandtl-Meyer expansion.[7] The process for calculating the new Mach number after the expansion requires that one first determine the angle ν_1. The angle ν_1 is the angle through which a flow at Mach 1 must be expanded to reach the freestream supersonic Mach number M_1, and is given by

$$\nu_1 = \sqrt{\frac{\gamma+1}{\gamma-1}}\tan^{-1}\sqrt{\frac{\gamma-1}{\gamma+1}(M_1^2-1)} - \tan^{-1}\sqrt{M_1^2-1} \tag{5}$$

The total angle ν_2 through which the flow is turned is $\nu_2 = \nu_1 + \delta$ where δ is the angle of the expansion ramp in radians. To determine the resulting Mach number after the expansion, M_2, the following equation must be solved numerically:

$$f(M_2) = \sqrt{\frac{\gamma+1}{\gamma-1}}\tan^{-1}\sqrt{\frac{\gamma-1}{\gamma+1}(M_2^2-1)} - \tan^{-1}\sqrt{M_2^2-1} - \nu_2 \tag{6}$$

Once the solution to Equation (6) is determined, the flow properties after the expansion are found from the thermodynamic relations for isentropic flow:

$$\frac{p_2}{p_1} = \left[\frac{1+\frac{\gamma-1}{2}M_1^2}{1+\frac{\gamma-1}{2}M_2^2}\right]^{\frac{\gamma}{\gamma-1}} \tag{7}$$

$$\frac{T_2}{T_1} = \left[\frac{1+\frac{\gamma-1}{2}M_1^2}{1+\frac{\gamma-1}{2}M_2^2}\right] \tag{8}$$

Prandtl-Meyer theory predicts that as $M_1 \to \infty$, the maximum angle through which the flow can be expanded is 130.4°. This implies that there are cases where the numerical solution of Equation 6 will not converge.

Once the downstream pressures are calculated according to either Oblique Shock Theory or Prandtl-Meyer Expansion Flow Theory, we can determine the aerodynamic forces acting on the vehicle. From Figure 3, the pressure on the lower forebody can be resolved into its x and z body axis components

$$F_{x,f} = -p_f L_f \tan \tau_{1\ell} \tag{9}$$

$$F_{z,f} = -p_f L_f \tag{10}$$

where L_f is the length of the forebody and p_f is the static pressure on the forebody. The pitching moment due to the forebody aerodynamic forces is

$$M_f = z_f \, F_{x,f} - x_f \, F_{z,f} \tag{11}$$

where (x_f, z_f) are the coordinates of the aerodynamic center of the lower forebody panel relative to the center-of-mass of the aircraft. The aerodynamic center occurs at the mid-point of the panel since the pressure distribution on the lower forebody is uniform behind the oblique shock wave.

Likewise, the pressures on the upper surface of the aircraft give the following body-axes forces and pitching moment

$$F_{x,u} = -p_u \, L_u \, \tan \tau_{1u} \tag{12}$$

$$F_{z,u} = p_u L_u \tag{13}$$

$$M_u = z_u \, F_{x,u} - x_u \, F_{z,u} \tag{14}$$

The length of the upper surface is L_u, the angle of the upper surface of the vehicle with respect to the x body axis is τ_{iu}, and the coordinates of the center of the upper surface panel relative to the center-of-mass are given by (x_u, z_u).

Scramjet Model

In the hypersonic flight regime, to produce the thrust necessary to maintain sustained flight one is limited to either rocket propulsion or supersonic combustion ramjet engines (scramjets). Whereas the ramjet slows the flow to subsonic speeds for combustion, the scramjet has supersonic flow in the combustion chamber. Around Mach 5, the losses that are experienced bringing the flow to subsonic conditions in the ramjet are significant and the scramjet becomes the more viable option for air-breathing propulsion. The primary advantage of the scramjet engine over the rocket engine is that it offers an opportunity for increased payload. Unlike the rocket engine, which requires that both the oxidizer and the fuel be carried on-board the vehicle, the scramjet only requires that the aircraft carry the fuel. Therefore, the volume that is dedicated to carrying an oxidizer for the rocket can now be used for payload. However, one downside of the scramjet is that it is only operable in the hypersonic regime (Mach numbers $\gtrapprox 5$). To overcome this, one concept that has been proposed is the rocket-based combined-cycle propulsion system that marries the rocket, ramjet, and scramjet engines.[8] This propulsion system accommodates all phases of flight from subsonic to supersonic to hypersonic to orbital.

The scramjet used for this model is shown in Figure 4 and is identical to that used by Chavez and Schmidt.[3] The conditions given at the engine inlet (station 1) are primarily determined by the Mach number and angle-of-attack at which the aircraft is flying. These parameters determine, in part, the properties of the bow shock. The flow through the diffuser is assumed to be isentropic (i.e., without loss). The two control variables that determine the thrust setting are the diffuser area ratio, A_d, and the heat addition in the combustion chamber, ΔT_0. Controlling A_d allows one to modulate the Mach number and the static pressure of the air entering into the combustion chamber. Ideally, the air will remain supersonic to avoid significant ram drag penalties. Because the air entering the combustor is supersonic, the heat release due to fuel combustion *reduces* the Mach number of the airstream that is passing through the engine. Care must be taken to ensure that too much heat is not added in order to prevent the flow through the engine from becoming thermally choked.

In the diffuser, we apply the continuity equation (conservation of mass) to determine the Mach number at the diffuser exit/combuster inlet (station 2) given the diffuser inlet Mach:

$$\frac{[1 + \frac{\gamma-1}{2} M_2^2]^{\frac{\gamma+1}{\gamma-1}}}{M_2^2} = A_d^2 \frac{[1 + \frac{\gamma-1}{2} M_1^2]^{\frac{\gamma+1}{\gamma-1}}}{M_1^2} \tag{15}$$

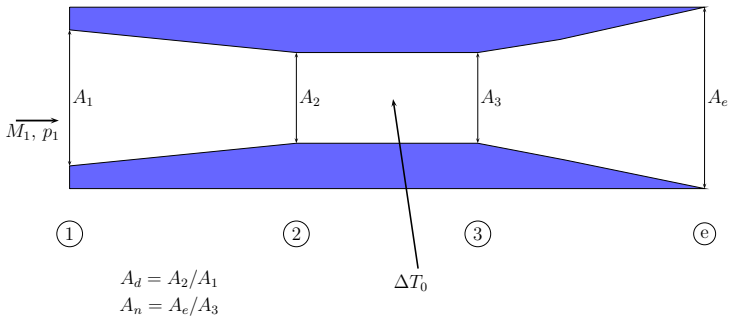

Figure 4. Scramjet Cross Section

The pressure and temperature at station 2 are determined by Equations (7) and (8).

The combustor is modelled as a constant-area, frictionless duct with heat addition. The Mach number at the combustor exit (station 3) is given by

$$\frac{M_3^2[1+\frac{1}{2}(\gamma-1)M_3^2]}{(\gamma M_3^2+1)^2} = \frac{M_2^2(1+\frac{1}{2}(\gamma-1)M_2^2)}{(\gamma M_2^2+1)^2} + \frac{M_2^2}{(\gamma M_2^2+1)^2}\frac{\Delta T_0}{T_2} \tag{16}$$

where ΔT_0 is the change in total temperature in the combustor due to the fuel burn. The pressure and temperature at the combustor exit are

$$p_3 = p_2\frac{1+\gamma M_2^2}{1+\gamma M_3^2} \tag{17}$$

$$T_3 = \frac{M_3^2}{M_2^2}\frac{(1+\gamma M_2^2)^2}{(1+\gamma M_1^2)^2} \tag{18}$$

The flow, upon leaving the combustor, enters a converging/diverging, isentropic nozzle that will ultimately increase the exit Mach number. The nozzle area ratio, A_n is assumed to be fixed. The exit Mach number is given by

$$\frac{[1+\frac{\gamma-1}{2}M_e^2]^{\frac{\gamma+1}{\gamma-1}}}{M_e^2} = A_n^2\frac{[1+\frac{\gamma-1}{2}M_3^2]^{\frac{\gamma+1}{\gamma-1}}}{M_3^2} \tag{19}$$

while the pressure and temperature at the exit plane are given by Equations (7) and (8).

The thrust is calculated by applying the Momentum Theorem from fluid mechanics to a control volume that encloses the scramjet engine. The thrust is given by

$$\mathcal{T} = \dot{m}_a(V_e - V_\infty) + (p_e - p_\infty)\frac{A_e}{b} - (p_1 - p_\infty)\frac{A_e/b}{A_n\,A_d} \tag{20}$$

where $\mathcal{T}$ is the engine thrust, $\dot{m}_a$ is the mass flow of air through the engine, V_e is the exit velocity of the air, V_∞ is the velocity of the freestream, p_e is the pressure at the exit plane of the engine, p_1 is the pressure at the engine inlet plane, p_∞ is the freestream pressure, A_e/b is the exit area per unit span, A_n is the nozzle area ratio, and A_d is the diffuser area ratio. It has been assumed that the mass flow of the fuel is negligible when compared to the mass flow of air.

An important parameter in the thrust equation, Equation (20) is the mass flow term, $\dot{m}_a$. The amount of mass flow captured by the engine inlet is a function of the shock angle, as shown in Figure 5. Typically, the aircraft geometry is designed with the intent to have the bow shock impinge upon the engine inlet lip at the design cruise condition. This will result in maximum mass flow through the engine module. At off-design conditions where the bow shock no longer impinges on the lip (cruise Mach less than the design Mach at the same angle-of-attack), there will be mass flow spillage as the shock will be positioned in front of the cowl lip. Therefore, we have added a translating cowl lip that can be positioned instantaneously to be coincident with

the bow shock. By positioning the cowl lip in such a manner, we can maximize the mass flow through the engine for any off-design flight condition. The penalty to be paid for this is that the lift, drag and pitching moment are affected by the length of the cowl lip. When the cowl lip intersects the shock, a second oblique shock occurs under the engine nacelle for positive angles-of-attack. For negative angles-of-attack, there is a Prandtl-Meyer Expansion Fan that turns the flow parallel to the nacelle. The pressure can be calculated using the methods given in the previous section. The only contribution is to the z-axis body force:

$$F_{z,n} = -p_n L_n \tag{21}$$

where p_n is the pressure on the bottom of the nacelle, and L_n is the length of the nacelle. The nacelle length L_n is the sum of the nominal nacelle length with the door completely retracted, L_{n0}, and the length of the translating lip $L_n = L_{n0} + L_{\text{door}}$. The length of the cowl door is

$$L_{\text{door}} = L_1 - (L_1 \tan \tau_{1\ell} + h_i) \cot(\theta_s - \alpha) \tag{22}$$

where h_i is as defined in Figure 3. The pitching moment created by $F_{z,n}$ is

$$M_n = -F_{z,n}[x_{n0} + \frac{1}{2}(L_{door} - L_{n0})] \tag{23}$$

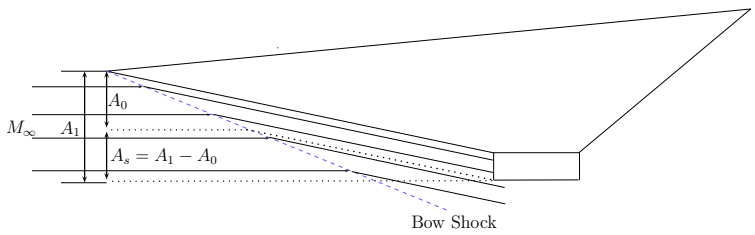

Figure 5. Capture Area/Mass Flow Spillage

Engine Inlet Turning Force

The airflow, after passing through the oblique shock, is parallel to the forebody; therefore, it must be turned parallel to the engine centerline. As a result, the force imparted by the air on the aircraft is

$$F_{x,\text{inlet}} = \gamma M_1^2 p_1 (1 - \cos(\tau_{1\ell} + \alpha)) \frac{A_e}{b} \frac{1}{A_d A_n} \tag{24}$$

$$F_{z,\text{inlet}} = \gamma M_1^2 p_1 \sin(\tau_{1\ell} + \alpha) \frac{A_e}{b} \frac{1}{A_d A_n} \tag{25}$$

$$M_{\text{inlet}} = z_{\text{inlet}} F_{x,\text{inlet}} - x_{\text{inlet}} F_{z,\text{inlet}} \tag{26}$$

where p_1 is the pressure after the bow shock, M_1 is the Mach number after the bow shock, and $(x_{\text{inlet}}, z_{\text{inlet}})$ is the location of the nominal inlet location relative to the center-of-mass. The mechanism for turning the flow axial to the engine is another oblique shock. There will be a resulting rise in static pressure and temperature with a decrease in Mach number as the flow crosses this shock. The new pressures and temperatures are calculated using the expressions given previously.

Aftbody Pressure

The pressure acting on the aftbody of the vehicle is due to the external expansion of the exhaust from the scramjet engine. The aftbody forms the upper part of a nozzle, while the shear layer that results from the interaction of the exhaust plume with the freestream flow forms the lower surface. The pressure distribution

along the aftbody is then is a function of the position of the shear layer. The shear layer is formed where the pressure in the plume is balanced by the freestream pressure. A reasonable approximation for the pressure at any point on the aftbody is given by Chavez and Schmidt[3]

$$p_a = \frac{p_e}{1 + x_a/L_a(p_e/p_\infty - 1)} \tag{27}$$

where L_a is the length of the aftbody panel as shown in Figure 3 and x_a is the distance along the aftbody panel.

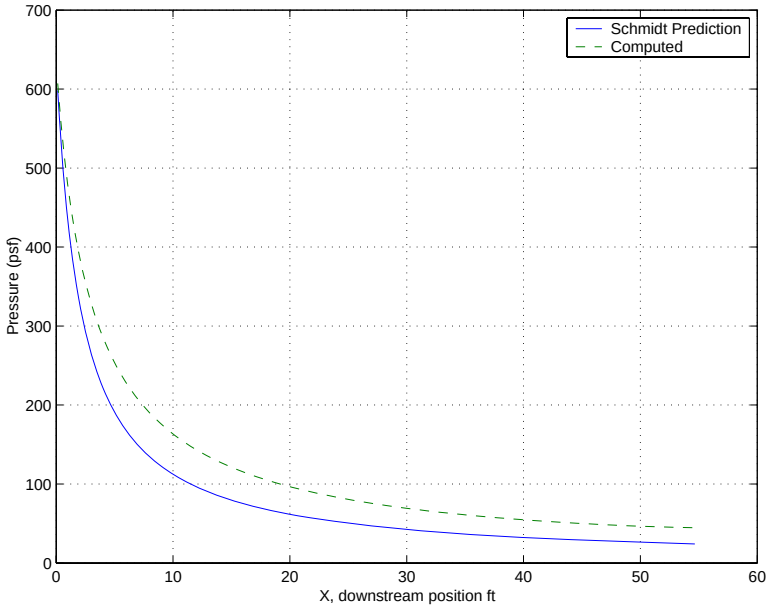

Figure 6. Comparison of Approximate and Exact Pressure Acting on the Aftbody of the HSV

A comparison of the approximate pressure, as given by Equation (27), to the pressure calculated after determining the exact position of the shear layer is given in Figure 6. It is readily evident that the approximation is of sufficient accuracy to model the aftbody pressure. The advantage of using Equation (27) is the computational efficiency that it affords, as the determination of the shear layer position requires a rather complicated algorithm.

The aftbody pressure makes a contribution to the lift and also acts to offset the drag of the forebody. The x and z body axis forces are

$$F_{x,a} = p_\infty L_a \frac{p_e}{p_\infty} \frac{\ln \frac{p_e}{p_\infty}}{\frac{p_e}{p_\infty} - 1} \tan(\tau_2 + \tau_{1,u}) \tag{28}$$

$$F_{z,a} = -p_\infty L_a \frac{p_e}{p_\infty} \frac{\ln \frac{p_e}{p_\infty}}{\frac{p_e}{p_\infty} - 1} \tag{29}$$

The pitching moment due to these forces is assumed to act at the mid-point of the aftbody panel

$$M_a = z_a\, F_{x,a} - x_a\, F_{z,a} \tag{30}$$

Here (x_a, z_a) are the coordinates of the mid-point of the aftbody relative to the center-of-mass of the vehicle.

Control Surface Model

As shown in Figure 3, there is a control surface available that helps to control the pitching moment acting on the aircraft along with lift and drag. The control surface is modelled as a flat plate that is hinged at its

mid-chord point so the entire surface deflects. The pressures on the upper and lower surfaces of the elevator are determined by the incidence of the control surface with the flow. In any case, on one side of the control surface, the pressure will determined by Prandtl-Meyer flow and the pressure on the second side will be determined by oblique shock theory. The resultant force acts at the mid-chord of the control surface. The x and z body forces,are

$$F_{x,c} = -(p_{c,\ell} - p_{c,u}) \sin(\delta_e)\, S_e \tag{31}$$
$$F_{z,c} = -(p_{c,\ell} - p_{c,u}) \cos(\delta_e)\, S_e \tag{32}$$
$$\tag{33}$$

The pressure on the upper surface is $p_{c,u}$, the pressure on the lower surface is $p_{c,\ell}$, δ_e is the control surface deflection relative to the freestream flow, and the area of the control surface is S_c. For the case where $\delta_e > 0$, $F_{z,c} < 0$ (the control surface is generating positive lift) and $F_{x,c} < 0$ (the drag due to the control surface being deflected acts opposite the x-body axis). On the other hand, if $\delta_e < 0$, we get $F_{x,c} < 0$ and $F_{z,c} > 0$ which is as expected.

The pitching moment due to the deflection of the control surface is

$$M_c = z_c\, F_{x,c} - x_c\, F_{z,c} \tag{34}$$

where (x_c, z_c) are the position of the midpoint of the control surface.

Once all of the forces and moments due to the aerodynamics have been determined, the resultant body forces and the moment are summed from the individual components. The forces are

$$F_x = \sum_{j=1}^{N} F_{x,j} \tag{35}$$
$$= F_{x,f} + F_{x,n} + F_{x,a} + F_{x,u} + F_{x,c} + F_{x,\text{inlet}} \tag{36}$$
$$F_z = \sum_{j=1}^{N} F_{z,j} \tag{37}$$
$$= F_{z,f} + F_{z,n} + F_{z,a} + F_{z,u} + F_{z,c} + F_{z,\text{inlet}} \tag{38}$$

The pitching moment is the sum of the forces acting on each component of the vehicle along with the pitching moment due to the engine thrust. From Figure 3, it is readily apparent that the thrust force has a profound influence on the pitching moment since it located well below the center-of-mass of the vehicle. The total moment acting on the vehicle is then

$$M = M_f + M_u + M_n + M_a + M_c + M_{\text{inlet}} + z_{\mathcal{T}}\mathcal{T} \tag{39}$$

The forces F_x and F_z can be translated into the lift and drag acting on the aircraft by using the following coordinate transformation

$$\mathcal{R}_\alpha = \begin{bmatrix} \cos\alpha & 0 & \sin\alpha \\ 0 & 1 & 0 \\ -\sin\alpha & 0 & \cos\alpha \end{bmatrix} \tag{40}$$

The rotation matrix $\mathcal{R}_\alpha$ carries the body axis frame to the stability axis. The stability axis system is aligned such that it x axis is coincident with the velocity vector. The lift and drag are then

$$L = F_x \sin\alpha - F_z \cos\alpha \tag{41}$$
$$D = -F_x \cos\alpha - F_z \sin\alpha \tag{42}$$

while the pitching moment remains unchanged.

Flexible Aircraft Model

For HSV type vehicles, flexibility effects play an important part in the aerodynamics of the aircraft. From the equations derived in the previous section, it is evident that the structural bending will have an effect on the angle of the bow shock, thereby affecting the pressures downstream of the shock. In particular, deflection of the forebody affects the thrust not only through changes in pressure due to the moving shock, but also through the effects of massflow spillage (assuming that there is no way to control the massflow through the engine.).

Vibrational Model

For the dynamic simulation, a vibrational model of the fuselage is necessary. The fuselage model is assumed to be comprised of two cantilever beams, one pointing forward and one aft, that are clamped at the center-of-mass of the fuselage. Thus, the root of each beam will rotate and translate according to the motion of the aircraft's center-of-mass. Only the transverse displacements of the beams are of interest, and it is assumed that the displacements are sufficiently small such that Hooke's Law is valid. We will denote the displacement and rotation of the forward beam with a subscript f and the displacement and rotation of the aft beam will be denoted with a subscript a.

It can be shown[9] that the transverse vibration of a cantilever beam with constant EI and constant mass density $\hat{m}$ satisfies the following partial-differential equation:

$$EI\frac{\partial^4 w(x,t)}{\partial x^4} + \hat{m}\frac{\partial^2 w(x,t)}{\partial t^2} = 0 \tag{43}$$

Assuming that the solution takes the form $w(x,t) = \phi(x)f(t)$, then Equation (43) can be separated into two ordinary differential equations:

$$EI\frac{d^4\phi(x)}{dx^4} - \omega^2\hat{m}\phi(x) = 0 \tag{44}$$

$$\frac{d^2 f(t)}{dt^2} + \omega^2 f(t) = 0 \tag{45}$$

Defining $\beta^4 = \omega^2\hat{m}/(EI)$, Equation (44) takes the form

$$\frac{d^4\phi(x)}{dx^4} - \beta^4\phi(x) = 0 \tag{46}$$

The solution to Equation (46) is

$$\phi(x) = A\sin\beta x + B\cos\beta x + C\sinh\beta x + D\cosh\beta x \tag{47}$$

For the forward-facing beam, we apply the following boundary conditions:

$$\phi_f(\bar{x}) = 0 \tag{48}$$

$$\phi_f'(\bar{x}) = 0 \tag{49}$$

$$\phi_f''(0) = 0 \tag{50}$$

$$\phi_f'''(0) = 0 \tag{51}$$

and we obtain the following frequency equation:

$$\cos\beta\bar{x}\cosh\beta\bar{x} = -1 \tag{52}$$

Equation (52) has an infinite number of solutions, β_k that can only be found through the application of numerical methods. The mode shapes for the forward beam corresponding to the frequencies can be shown to be

$$\begin{aligned}\phi_{f,k}(x) = A_{f,k}[&(\sin\beta_{f,k}\bar{x} - \sinh\beta_{f,k}\bar{x})(\sin\beta_{f,k}x + \sinh\beta_{f,k}x)\\ &+ (\cos\beta_{f,k}\bar{x} + \cosh\beta_{f,k}\bar{x})(\cos\beta_{f,k}x + \cosh\beta_{f,k}x)]\end{aligned} \tag{53}$$

The mode shapes $\phi_{f,k}(x)$ form an orthogonal set of solutions and we choose the value of $A_{f,k}$ such that

$$\int_0^{\bar{x}} \hat{m}\phi_{f,j}(x)\phi_{f,k}(x)\,dx = \begin{cases} 0 & \text{if} \quad j \neq k \\ 1 & \text{if} \quad j = k \end{cases} \tag{54}$$

For the aft beam, the boundary conditions are

$$\phi_a(0) = 0 \tag{55}$$
$$\phi_a'(0) = 0 \tag{56}$$
$$\phi_a''(L-\bar{x}) = 0 \tag{57}$$
$$\phi_a'''(L-\bar{x}) = 0 \tag{58}$$

Although the fixed end of the beam is at the center-of-mass, we have defined the boundary conditions such that the beam is of length $L - \bar{x}$ and the clamped end is at the origin. Applying the boundary conditions results in the same frequency equation as before (Equation (52)). The corresponding mode shape, written on the domain $x \in [\bar{x}, L]$ is

$$\begin{aligned} \phi_{a,k}(x) = A_{a,k}[&(\sin\beta_{a,k}(L-\bar{x}) - \sinh\beta_{a,k}(L-\bar{x}))(\sin\beta_{a,k}(x-\bar{x}) - \sinh\beta_{a,k}(x-\bar{x})) \\ &+ (\cos\beta_{a,k}(L-\bar{x}) + \cosh\beta_{a,k}(L-\bar{x}))(\cos\beta_{a,k}(x-\bar{x}) - \cosh\beta_{a,k}(x-\bar{x}))] \end{aligned} \tag{59}$$

The mode shapes $\phi_{a,k}(x)$ also form a mass-normalized, orthogonal set of solutions.

The displacement and slope of the beam, determined from the mode shapes above, are shown in Figure 7

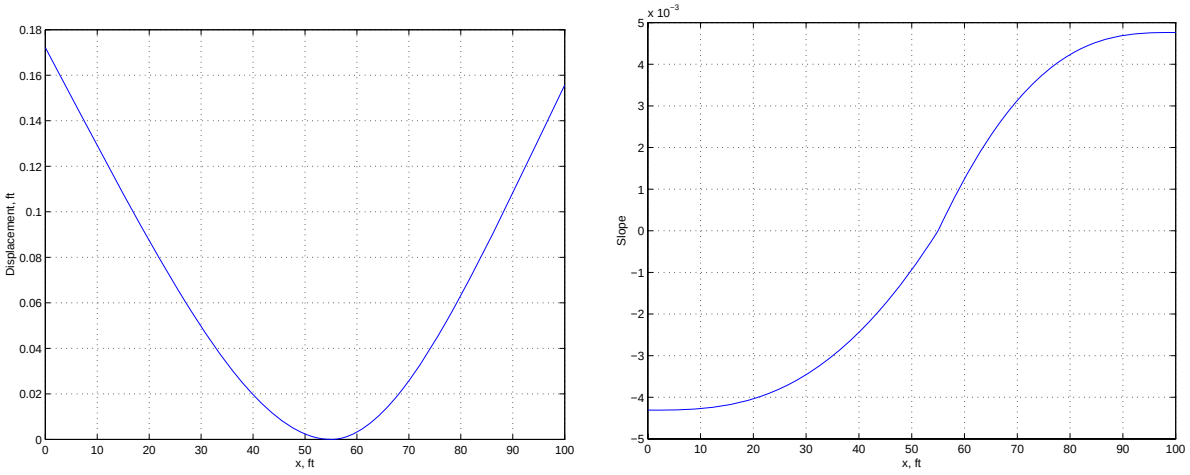

(a) Fuselage Displacement

(b) Fuselage Rotation

Figure 7. Beam Mode Shape

Forced Response

For the case where there are distributed and concentrated loads on the beam, Equation (43) becomes

$$EI\frac{\partial^4 w(x,t)}{\partial x^4} + \hat{m}\frac{\partial^2 w(x,t)}{\partial t^2} = p(x,t) + P_j(t)\boldsymbol{\delta}(x - x_j) \tag{60}$$

From the expansion theorem, the solution of Equation (60) is

$$w(x,t) = \sum_{k=1}^{\infty} \phi_k(x)\eta_k(t) \tag{61}$$

where $\eta_k(t)$ is the generalized modal coordinate. It can be shown that η_k satisfies the differential equation[10]

$$\ddot{\eta}_k + \omega_k^2 \eta_k = N_k(t) \tag{62}$$

where the generalized modal force associated with the k^{th} mode shape is

$$N_k(t) = \int_0^L \phi_k(x) p(x,t)\, dx + \sum_{j=1}^{l} \phi(x_j) P_j(t) \tag{63}$$

In Equation (63), l is the number of concentrated forces applied to the beam. The solution to Equation (62) for the k^{th} frequency is[10]

$$\eta_k(t) = \frac{1}{\omega_k} \int_0^t N_k(\tau) \sin(\omega_k(t-\tau))\, d\tau + \eta_k(0) \cos \omega_k t + \dot{\eta}_k(0) \frac{\sin \omega_k t}{\omega_k} \tag{64}$$

The initial conditions $\eta_k(0)$ and $\dot{\eta}_k(0)$ are given by Meirovitch [10] as

$$\eta_k(0) = \int_0^L \hat{m} \phi_k(x) w(x,0)\, dx \tag{65}$$

$$\dot{\eta}_k(0) = \int_0^L \hat{m} \phi_k(x) \dot{w}(x,0)\, dx \tag{66}$$

Lagrange's Equations for a Flexible Aircraft

In this section, we focus on the derivation of the equations of motion for a flexible aircraft. There are several approaches in the literature that discuss the determination of the equations-of-motion for a flexible aircraft. Bisplinghoff and Ashley derive the equations-of-motion for an "unconstrained vehicle." They show that the rigid body and the vibrational mode shapes are orthogonal. Waszak and Schmidt,[11] use a "mean elastic axis" that physically decouples the rigid-body equations and the equations of motion that describe the vibration of the aircraft. In both the Waszak and Bisplinghoff models, the coupling of the rigid body rotation and translation with the structural modes is implicit as the effects of the bending are only present in the forces and moments. This means that the mean axis assumption does not capture the inherent coupling between the aircraft's pitch acceleration, the aircraft's normal acceleration, and the transverse vibration of the aircraft. Papers by Olsen[12] and Buttrill, et.al.[13] each take into account the coupling between the aircraft's linear and angular accelerations with the elastic modes. Olsen makes no assumption on how the mode shapes are represented, while Buttrill assumes a lumped-mass approach. Finally, Meirovitch and Tuzcu[14] give another approach that attempts unify the disciplines of dynamics, controls, aeroelasticity, and aerodynamics. Meirovitch gives a rather lengthy argument against the use of mean elastic axes and for the need to ensure that the rigid-body and elastic mode coupling is present. Meirovitch then presents a derivation of the equations-of-motion for an elastic aircraft based upon Lagrange's Equations. The approach that we take most closely follows that of Meirovitch.

For our derivation of the equations-of-motion, we will assume that there are no torsional vibrations, no longitudinal or "pogo" vibrations, and that the mass of the aircraft is constant. To derive the equations-of-motion for this system, we shall use Lagrange's Equations. Recall that the Lagrangian is defined as $\mathscr{L} = T - V$ where T is the kinetic energy of the system and V is the potential energy. If we assume that there are n generalized coordinates, q_i, then Lagrange's Equations are

$$\frac{d}{dt}\frac{\partial \mathscr{L}}{\partial \dot{q}_i} - \frac{\partial \mathscr{L}}{\partial q_i} = Q_i, \quad i = 1, \ldots, n \tag{67}$$

where Q_i is the generalized force associated with generalized coordinate q_i. The generalized force can be either a force or moment, depending upon whether the generalize coordinate q_i represents a translation or rotation. The generalized forces are determined from the following equation for the virtual work due to non-conservative forces:

$$\delta W = \sum_{i=1}^{n} Q_i \delta q_i \tag{68}$$

where δq_i is the variation of the i^{th} generalized coordinate. Alternatively, the i^{th} generalized force can be determined from $Q_i = \sum_{i=1}^{N} \boldsymbol{f}_i \cdot \partial \boldsymbol{r} / \partial q_r$ where $\boldsymbol{f}_i$ is the i^{th} applied non-conservative force and N is the number of non-conservative forces applied to the body.

Let $\boldsymbol{r}_P(t)$ denote the position of a point P in a *flexible* body. We can express this position in terms of the inertial position of the center-of-mass, $\boldsymbol{r}_0(t)$ and the position of P relative to the center-of-mass in some set of body-fixed axes, $\boldsymbol{r}_{P/0}(t)$.

$$\boldsymbol{r}_P(t) = \boldsymbol{r}_0(t) + \boldsymbol{r}_{P/0}(t) \tag{69}$$

where

$$\boldsymbol{r}_{P/0} = \boldsymbol{\rho}(t) + \boldsymbol{d}(t) \tag{70}$$

In Equation (70), $\boldsymbol{\rho}$ is the position of the point P in the undeformed body (i.e., if the body were perfectly rigid) and is written in the body-fixed axes. The vector $\boldsymbol{d}$ denotes the position of point P relative to its undeformed position and is also written in terms of the body axes.

To find the velocity of the point P, we differentiate Equation (69)

$$\dot{\boldsymbol{r}}_P(t) = \dot{\boldsymbol{r}}_0 + \frac{\delta \boldsymbol{r}_{P/0}}{\delta t} + \boldsymbol{\omega} \times \boldsymbol{r}_{P/0} \tag{71}$$

where $\delta \boldsymbol{r}_{P/0} / \delta t$ denotes that portion of the total derivative that involves only the derivatives of the components in the body frame (i.e., $\delta \boldsymbol{r}_{P/0} / \delta t$ is the time rate-of-change of $\boldsymbol{r}_{P/0}$ as seen by an observer who is fixed in the body frame):

$$\frac{\delta \boldsymbol{r}_{P/0}}{\delta t} = \dot{x}\, \boldsymbol{e}_1 + \dot{y}\, \boldsymbol{e}_2 + \dot{z}\, \boldsymbol{e}_3 \tag{72}$$

We then form the kinetic energy:

$$T = \frac{1}{2} \int_{\boldsymbol{B}} \dot{\boldsymbol{r}}_p \cdot \dot{\boldsymbol{r}}_p \, dm \tag{73}$$

If we substitute Equations (71) and (70) into the Equation (73) we get

$$\begin{aligned} T = \frac{1}{2} \int_{\boldsymbol{B}} & \dot{\boldsymbol{r}}_0 \cdot \dot{\boldsymbol{r}}_0 + (\boldsymbol{\omega} \times \boldsymbol{\rho}) \cdot (\boldsymbol{\omega} \times \boldsymbol{\rho}) + (\boldsymbol{\omega} \times \boldsymbol{d}) \cdot (\boldsymbol{\omega} \times \boldsymbol{d}) + \\ & \frac{\delta \boldsymbol{d}}{\delta t} \cdot \frac{\delta \boldsymbol{d}}{\delta t} + 2 \Bigg(\dot{\boldsymbol{r}}_0 \cdot (\boldsymbol{\omega} \times \boldsymbol{\rho}) + \dot{\boldsymbol{r}}_0 \cdot (\boldsymbol{\omega} \times \boldsymbol{d}) + \dot{\boldsymbol{r}} \cdot \frac{\delta \boldsymbol{d}}{\delta t} + \\ & (\boldsymbol{\omega} \times \boldsymbol{\rho}) \cdot (\boldsymbol{\omega} \times \boldsymbol{d}) + (\boldsymbol{\omega} \times \boldsymbol{\rho}) \cdot \frac{\delta \boldsymbol{d}}{\delta t} + (\boldsymbol{\omega} \times \boldsymbol{d}) \cdot \frac{\delta \boldsymbol{d}}{\delta t} \Bigg) \, dm \end{aligned} \tag{74}$$

We recognize the first term in Equation (74) as the kinetic energy due to the translation of the center-of-mass: $T_{\text{trans}} = (1/2)\, m \dot{\boldsymbol{r}}_0 \cdot \dot{\boldsymbol{r}}_0$. The second term is the kinetic energy due to the rotation of the undeformed body about its center-of-mass: $T_{\text{rot}} = (1/2)\, \boldsymbol{\omega} \cdot I \boldsymbol{\omega}$. Making these substitutions, Equation (74) takes the form:

$$\begin{aligned} T = \frac{1}{2}\, m\, \dot{\boldsymbol{r}}_0 \cdot \dot{\boldsymbol{r}}_0 + \frac{1}{2}\, \boldsymbol{\omega} \cdot I \boldsymbol{\omega} + \frac{1}{2} \int_B & (\boldsymbol{\omega} \times \boldsymbol{d}) \cdot (\boldsymbol{\omega} \times \boldsymbol{d}) + \\ & \frac{\delta \boldsymbol{d}}{\delta t} \cdot \frac{\delta \boldsymbol{d}}{\delta t} + 2 \Bigg(\dot{\boldsymbol{r}}_0 \cdot (\boldsymbol{\omega} \times \boldsymbol{\rho}) + \dot{\boldsymbol{r}}_0 \cdot (\boldsymbol{\omega} \times \boldsymbol{d}) + \dot{\boldsymbol{r}} \cdot \frac{\delta \boldsymbol{d}}{\delta t} + \\ & (\boldsymbol{\omega} \times \boldsymbol{\rho}) \cdot (\boldsymbol{\omega} \times \boldsymbol{d}) + (\boldsymbol{\omega} \times \boldsymbol{\rho}) \cdot \frac{\delta \boldsymbol{d}}{\delta t} + (\boldsymbol{\omega} \times \boldsymbol{d}) \cdot \frac{\delta \boldsymbol{d}}{\delta t} \Bigg) \, dm \end{aligned} \tag{75}$$

The terms that remain in the integrand are those that arise due to the elasticity of the aircraft.

We now turn our attention to the remaining terms in the integrand and the determination of their contribution to the kinetic energy. Note that the terms remaining in the integrand, with the exception of the first two terms, indicate a significant coupling between the rigid body and the elastic modes. In order

to evaluate the contributions of the aircraft's elasticity to the remaining kinetic energy terms, $\boldsymbol{d}$ is written in terms of the mode shapes of the body and the modal coordinates using the Expansion Theorem[9]

$$\boldsymbol{d} = \sum_{i=1}^{\infty} \phi_{y,i}(u,v,w)\eta_{y,i}(t)\boldsymbol{e}_2 + \sum_{i=1}^{\infty} \phi_{z,i}(u,v,w)\eta_{z,i}(t)\boldsymbol{e}_3 \tag{76}$$

and $\delta\boldsymbol{d}/\delta t$ is subsequently written as

$$\frac{\delta \boldsymbol{d}}{\delta t} = \sum_{i=1}^{\infty} \phi_{y,i}\dot{\eta}_{y,i}\boldsymbol{e}_2 + \sum_{i=1}^{\infty} \phi_{z,i}\dot{\eta}_{z,i}\boldsymbol{e}_3 \tag{77}$$

where the mode shapes are given by $\phi_{y,i}(u,v,w),$ and $\phi_{z,i}(u,v,w)$ and (u,v,w) are the spatial coordinates, in the $\boldsymbol{e}$-frame, of the elemental masses making up the body. Also note that ϕ_y is the mode shape of the lateral vibration, and ϕ_z is the mode shape of the transverse or normal vibration. The modal coordinates of the i^{th} mode shape are given by $\eta_{x,i}$, $\eta_{y,i}$ and $\eta_{z,i}$. The mode shapes for a given modal coordinate are orthogonal and mass-normalized such that

$$\int_B \phi_{z,i}\phi_{z,j}\, dm = \begin{cases} 0, & i \neq j \\ 1, & i = j \end{cases} \tag{78}$$

We will also assume that

$$\int_B \phi_{y,i}\phi_{z,j}\, dm = 0, \forall\, (i,j) \tag{79}$$

We continue our evaluation of the kinetic energy by considering the first term in the integrand:

$$\int_B (\boldsymbol{\omega} \times \boldsymbol{d}) \cdot (\boldsymbol{\omega} \times \boldsymbol{d})\, dm \tag{80}$$

Let $\boldsymbol{\omega} = P\boldsymbol{e}_1 + Q\boldsymbol{e}_2 + R\boldsymbol{e}_3$, and for the time being, let $\boldsymbol{d} = d_y\boldsymbol{e}_2 + d_z\boldsymbol{e}_3$. Expanding the integrand gives:

$$\int_B P^2(d_y^2 + d_z^2) + Q^2 d_z^2 + R^2 d_y^2 - 2QRd_y d_z\, dm \tag{81}$$

However,the angular rates are independent of the spatial coordinates (u,v,w) since all points in the body have the same angular velocity; therefore, the angular rates P, Q, R can be taken outside the integral. Making use of the fact that the mode shapes are orthogonal, Equation (81) becomes

$$P^2 \sum_{i=1}^{\infty}(\eta_{y,i}^2 + \eta_{z,i}^2) + Q^2 \sum_{i=1}^{\infty} \eta_{z,i}^2 + R^2 \sum_{i=1}^{\infty} \eta_{y,i}^2 - 2QR \sum_{i=1}^{\infty}\sum_{j=1}^{\infty} S_{yz}^{(i,j)}\eta_{y,i}\eta_{z,j} \tag{82}$$

where

$$S_{yz}^{(i,j)} = \int_B \phi_{y,i}\phi_{z,j}\, dm \tag{83}$$

The term $S_{yz}^{(i,j)}\eta_{y,i}\eta_{z,j}$ is the change in I_{yz} due to the deformation of the elastic aircraft.

Next, we evaluate the term

$$\int_B \frac{\delta \boldsymbol{d}}{\delta t} \cdot \frac{\delta \boldsymbol{d}}{\delta t}\, dm \tag{84}$$

From Equation (77), the integral becomes

$$\int_B \left(\sum_{i=1}^{\infty} \phi_{y,i}\dot{\eta}_{y,i}\right)^2 + \left(\sum_{i=1}^{\infty} \phi_{z,i}\dot{\eta}_{z,i}\right)^2 dm \tag{85}$$

Recalling that the mode shapes are mass-normalized and orthogonal, we get the following expression for the kinetic energy due to the bending of the fuselage:

$$\sum_{i=1}^{\infty}(\dot{\eta}_{y,i}^2 + \dot{\eta}_{z,i}^2) \tag{86}$$

The remaining terms in the kinetic energy expression that are to be evaluated are due to the interaction of the rigid body modes and the elastic modes. Under certain assumptions, these terms can vanish. Since we are interested in the most general case, we will include the remaining terms. Examining the term

$$\int_B \dot{\boldsymbol{r}}_0 \cdot (\boldsymbol{\omega} \times \boldsymbol{\rho})\, dm \tag{87}$$

and applying the vector triple product identity $\boldsymbol{a} \cdot (\boldsymbol{b} \times \boldsymbol{c}) = \boldsymbol{c} \cdot (\boldsymbol{a} \times \boldsymbol{b}) = \boldsymbol{b} \cdot (\boldsymbol{c} \times \boldsymbol{a})$ to this integral gives

$$(\dot{\boldsymbol{r}}_0 \times \boldsymbol{\omega}) \cdot \int_B \boldsymbol{\rho}\, dm = 0 \tag{88}$$

where $\int_B \boldsymbol{\rho}\, dm = 0$ is the center-of-mass in the body frame coordinates.

For the next term in the integrand, $\int_B \dot{\boldsymbol{r}}_0 \cdot (\boldsymbol{\omega} \times \boldsymbol{d})\, dm$, applying the vector triple product identity gives

$$(\dot{\boldsymbol{r}}_0 \times \boldsymbol{\omega}) \cdot \int_B \boldsymbol{d}\, dm \tag{89}$$

From the definition of $\boldsymbol{d}$

$$(\dot{\boldsymbol{r}}_0 \times \boldsymbol{\omega}) \cdot \int_B \sum_{i=1}^{\infty} \phi_{y,i}\eta_{y,i}\boldsymbol{e}_2 + \sum_{i=1}^{\infty} \phi_{z,i}\eta_{z,i}\boldsymbol{e}_3\, dm \tag{90}$$

Defining $\lambda_{y,i} = \int_B \phi_{y,i}\, dm$ and $\lambda_{z,i} = \int_B \phi_{z,i}\, dm$ gives

$$(\dot{\boldsymbol{r}}_0 \times \boldsymbol{\omega}) \cdot \left(\sum_{i=1}^{\infty} \lambda_{y,i}\eta_{y,i}\boldsymbol{e}_2 + \lambda_{z,i}\eta_{z,i}\boldsymbol{e}_3 \right) \tag{91}$$

We leave the evaluation of the cross-product $\dot{\boldsymbol{r}}_0 \times \boldsymbol{\omega}$ for later.

The next term in the kinetic energy, $\int_B \dot{\boldsymbol{r}}_0 \cdot \delta\boldsymbol{d}/\delta t\, dm$ can be written using the definitions for $\lambda_{y,i}$ and $\lambda_{z,i}$ and $\delta\boldsymbol{d}/\delta t$ as

$$\dot{\boldsymbol{r}}_0 \cdot \left(\sum_{i=1}^{\infty} \lambda_{y,i}\dot{\eta}_{y,i}\boldsymbol{e}_2 + \lambda_{z,i}\dot{\eta}_{z,i}\boldsymbol{e}_3 \right) \tag{92}$$

Again, we delay complete evaluation of the term until later.

The term, $\int_B (\boldsymbol{\omega} \times \boldsymbol{\rho}) \cdot (\boldsymbol{\omega} \times \boldsymbol{d})\, dm$ becomes

$$\begin{aligned} P^2 \sum_{i=1}^{\infty} (\sigma_{y,i}\eta_{y,i} + \sigma_{z,i}\eta_{z,i}) + Q^2 \sum_{i=1}^{\infty} \sigma_{z,i}\eta_{z,i} + R^2 \sum_{i=1}^{\infty} \sigma_{y,i}\eta_{y,i} - \\ QR \sum_{i=1}^{\infty} (\psi_{yz,i}\eta_{z,i} + \psi_{zy,i}\eta_{y,i}) - PR \sum_{i=1}^{\infty} \psi_{xz,i}\eta_{z,i} + -PQ \sum_{i=1}^{\infty} \psi_{xy,i}\eta_{y,i} \end{aligned} \tag{93}$$

where $\psi_{xz,i} = \int_B u\phi_{z,i}\, dm$, $\psi_{zy,i} = \int_B w\phi_{y,i}\, dm$, etc. and $\sigma_{z,i} = \int_B w\phi_{z,i}\, dm$.

The term $\int_B (\boldsymbol{\omega} \times \boldsymbol{\rho}) \cdot \delta\boldsymbol{d}/\delta t\, dm$ can be determined using the previous definitions for $\psi_{xy,i}$, $\psi_{zy,i}$, etc.

$$\int_B (\boldsymbol{\omega} \times \boldsymbol{\rho}) \cdot \frac{\delta \boldsymbol{d}}{\delta t}\, dm = \sum_{i=1}^{\infty} (R\psi_{xy,i} - P\psi_{zy,i})\dot{\eta}_{y,i} + \sum_{i=1}^{\infty} (-Q\psi_{xz,i} + P\psi_{yz,i})\dot{\eta}_{z,i} \tag{94}$$

The final term in the kinetic energy expression can be shown to be

$$\int_B \frac{\delta \boldsymbol{d}}{\delta t} \cdot (\boldsymbol{\omega} \times \boldsymbol{d})\, dm = P \sum_{i=1}^{\infty} \sum_{j=1}^{\infty} S_{yz}^{(i,j)} (\dot{\eta}_{y,i}\eta_{z,j} - \eta_{y,i}\dot{\eta}_{z,j}) \tag{95}$$

Note that under certain assumptions, Equation (95) will become zero.

The total kinetic energy of elastic vehicle may now be written using the expressions given in Equations (82)-(95):

$$
\begin{aligned}
T = {} & \frac{1}{2}m\dot{\boldsymbol{r}}_0 \cdot \dot{\boldsymbol{r}}_0 + \frac{1}{2}\boldsymbol{\omega} \cdot I\boldsymbol{\omega} + \frac{1}{2}\sum_{i=1}^{\infty}(\dot{\eta}_{x,i}^2 + \dot{\eta}_{y,i}^2 + \dot{\eta}_{z,i}^2) + \frac{1}{2}P^2\sum_{i=1}^{\infty}(\eta_{y,i}^2 + \eta_{z,i}^2) + \\
& \frac{1}{2}Q^2\sum_{i=1}^{\infty}\eta_{z,i}^2 + \frac{1}{2}R^2\sum_{i=1}^{\infty}\eta_{y,i}^2 - QR\sum_{i=1}^{\infty}\sum_{j=1}^{\infty}S_{yz}^{(i,j)}\eta_{y,i}\eta_{z,j} + \\
& (\dot{\boldsymbol{r}}_0 \times \boldsymbol{\omega}) \cdot \sum_{i=1}^{\infty}(\lambda_{y,i}\eta_{y,i}\boldsymbol{e}_2 + \lambda_{z,i}\eta_{z,i}\boldsymbol{e}_3) + \dot{\boldsymbol{r}}_0 \cdot \left(\sum_{i=1}^{\infty}\lambda_{y,i}\dot{\eta}_{y,i}\boldsymbol{e}_2 + \lambda_{z,i}\dot{\eta}_{z,i}\boldsymbol{e}_3\right) + \\
& P^2\sum_{i=1}^{\infty}(\sigma_{y,i}\eta_{y,i} + \sigma_{z,i}\eta_{z,i}) + Q^2\sum_{i=1}^{\infty}\sigma_{z,i}\eta_{z,i} + R^2\sum_{i=1}^{\infty}\sigma_{y,i}\eta_{y,i} - \\
& QR\sum_{i=1}^{\infty}(\psi_{yz,i}\eta_{z,i} + \psi_{zy,i}\eta_{y,i}) - PR\sum_{i=1}^{\infty}\psi_{xz,i}\eta_{z,i} - PQ\sum_{i=1}^{\infty}\psi_{xy,i}\eta_{y,i} + \\
& \sum_{i=1}^{\infty}((R\psi_{xy,i} - P\psi_{zy,i})\dot{\eta}_{y,i} + (-Q\psi_{yz,i} + P\psi_{xz,i})\dot{\eta}_{z,i} + P\sum_{i=1}^{\infty}\sum_{j=1}^{\infty}S_{yz}^{(i,j)}(\dot{\eta}_{y,i}\eta_{z,j} - \eta_{y,i}\dot{\eta}_{z,j})
\end{aligned}
\tag{96}
$$

The potential energy of the body is comprised of the strain energy and the gravitational potential. We write the potential due to gravity as

$$V_g = -m\boldsymbol{g} \cdot \boldsymbol{r}_0 \tag{97}$$

and the strain energy is

$$V_s = -\frac{1}{2}\int_B \frac{\delta^2\boldsymbol{d}}{\delta t^2} \cdot \boldsymbol{d}\, dm \tag{98}$$

Substituting for $\delta^2\boldsymbol{d}/\delta t^2$,the strain energy becomes

$$
\begin{aligned}
V_s = {} & -\frac{1}{2}\int_B (\sum_{i=1}^{\infty}\phi_{y,i}\ddot{\eta}_{y,i}\boldsymbol{e}_2 + \sum_{i=1}^{\infty}\phi_{z,i}\ddot{\eta}_{z,i}\boldsymbol{e}_3) \cdot \\
& (\sum_{i=1}^{\infty}\phi_{x,i}\eta_{x,i}\boldsymbol{e}_1 + \sum_{i=1}^{\infty}\phi_{y,i}\eta_{y,i}\boldsymbol{e}_2 + \sum_{i=1}^{\infty}\phi_{z,i}\eta_{z,i}\boldsymbol{e}_3)\, dm \\
= {} & -\frac{1}{2}\int_B \sum_{i=1}^{\infty}\sum_{i=1}^{\infty}\phi_{y,i}^2\ddot{\eta}_{y,i}\eta_{y,i} + \sum_{i=1}^{\infty}\phi_{z,i}^2\ddot{\eta}_{z,i}\eta_{z,i}\, dm
\end{aligned}
\tag{99}
$$

Recognizing that the strain energy (i.e., stiffness) is independent of the loading on the body (see Reference 11), then the following substitution can be made: $\ddot{\eta}_i = -\omega_i^2\eta_i$ where ω_i is the natural frequency of the i^{th} mode shape. As a result, the strain energy becomes

$$V_s = \frac{1}{2}\sum_{i=1}^{\infty}(\omega_{y,i}^2\eta_{y,i}^2 + \omega_{z,i}^2\eta_{z,i}^2) \tag{100}$$

Finally, the potential energy can be written as:

$$V = -m\boldsymbol{g} \cdot \boldsymbol{r}_0 + \frac{1}{2}\sum_{i=1}^{\infty}(\omega_{y,i}^2\eta_{y,i}^2 + \omega_{z,i}^2\eta_{z,i}^2) \tag{101}$$

From this point forward, the determination of the equations-of-motion using Lagrange's Equations for the flexible aircraft is straight-forward since one is now left with taking derivatives of the Lagrangian with respect to q_i and $\dot{q}_i$ and any subsequent algebraic simplification.

Application of Lagrange's Equations to the Determination of the Longitudinal Equations of Motion for a Deformable Aircraft

Now we want to address the derivation of the equations-of-motion for the longitudinal dynamics of a flexible aircraft. The structural model is assumed to consist of two cantilever beams fixed at the origin. One reason for choosing this particular structural model was due to the fact that there was no available finite element model of the vehicle structure. In addition, this particular choice for the elastic structure captures the coupling between the pitch attitude and the normal acceleration with the elastic modes. The first beam will point towards the nose of the vehicle and the second will point towards the tail. Each beam will be assumed to deflect only in the z body-axis direction and the length of each beam will be assumed to be much larger than the thickness (i.e., neglect any rotatory inertia effects). Furthermore, the deflections are assumed to be small enough such that Hooke's Law is valid. As will be evident, these assumptions greatly simplify the kinetic energy term given by Equation 96.

The inertial frame will be denoted by the unit vector triad $(\boldsymbol{n}_1, \boldsymbol{n}_2, \boldsymbol{n}_3)$, and the body-axes frame unit vectors will be denoted by $(\boldsymbol{e}_1, \boldsymbol{e}_2, \boldsymbol{e}_3)$. The inertial frame is oriented such that $\boldsymbol{n}_1$ points north, $\boldsymbol{n}_2$ points east, and $\boldsymbol{n}_3 = \boldsymbol{n}_1 \times \boldsymbol{n}_2$ is positive down. The body-axes are oriented in the vehicle with $\boldsymbol{e}_1$ positive out the nose, $\boldsymbol{e}_2$ positive out the right wing. The unit vector $\boldsymbol{e}_3 = \boldsymbol{e}_1 \times \boldsymbol{e}_2$ is positive out the bottom of the aircraft. Both sets of unit vectors form orthogonal triads.

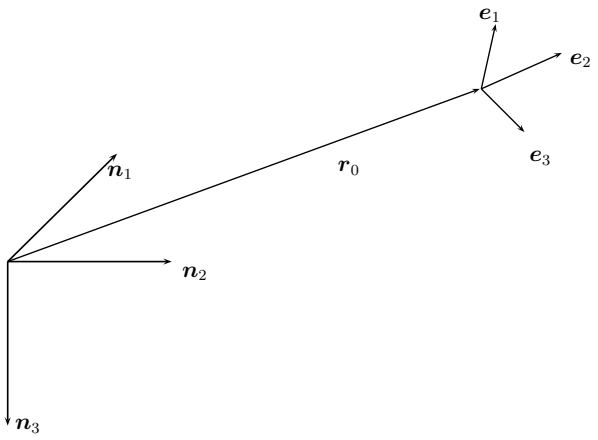

Figure 8. Inertial and Body-Fixed Reference Frames

It is also assumed that the aircraft is flying wings level (no roll) and without sideslip so the longitudinal and lateral-directional equations decouple. The $\boldsymbol{n}$ frame is carried into the $\boldsymbol{e}$ frame by the coordinate transformation:

$$\mathcal{R}_\theta = \begin{bmatrix} \cos\theta & 0 & -\sin\theta \\ 0 & 1 & 0 \\ \sin\theta & 0 & \cos\theta \end{bmatrix} \tag{102}$$

The angular velocity of the aircraft is $\boldsymbol{\omega} = Q\boldsymbol{e}_2 = \dot{\theta}\boldsymbol{n}_2$. However, from the definition of $\mathcal{R}_\theta$, it is evident that $Q = \dot{\theta}$.

The position of the center-of-mass is given in the $\boldsymbol{n}$ frame as $\boldsymbol{r}_0 = X\boldsymbol{n}_1 + Z\boldsymbol{n}_3$ and in the $\boldsymbol{e}$ frame as: $\boldsymbol{r}_0 = x\boldsymbol{e}_1 + z\boldsymbol{e}_2 = (X\cos\theta - Z\sin\theta)\boldsymbol{e}_1 + (X\sin\theta + Z\cos\theta)\boldsymbol{e}_2$. The velocity of the center-of-mass in the $\boldsymbol{e}$ frame is $\dot{\boldsymbol{r}}_0 = \delta\boldsymbol{r}_{P/0}/\delta t + \boldsymbol{\omega} \times \boldsymbol{r}_{P/0} = (\dot{x} + Qz)\boldsymbol{e}_1 + (\dot{z} - Qx)\boldsymbol{e}_2 = U\boldsymbol{e}_1 + W\boldsymbol{e}_2$

For the elastic modes of the aircraft, we are only interested in the first fuselage bending mode. The elastic deformation of the fuselage is modelled by two cantilever beams that are fixed at the center-of-mass such that they have no rotation or displacement relative to the center-of-mass. It is assumed that height of the beam is negligible as compared to the length so that $\boldsymbol{\rho} = u\boldsymbol{e}_1$ and $\boldsymbol{d} = d\boldsymbol{e}_3$. We denote the modal coordinates

of the beams as η_f and η_a respectively. The displacement of each beam can be written as $d_f = \sum_{i=1}^{\infty} \phi_{f,i}\eta_{f,i}$ and $d_a = \sum_{i=1}^{\infty} \phi_{a,i}\eta_{a,i}$.

We can now write the kinetic energy of the aircraft:

$$\begin{aligned} T = \frac{1}{2}m\Big[(\dot{x}+Qz)^2+(\dot{z}-Qx)^2)\Big] + \frac{1}{2}I_{yy}Q^2 + \frac{1}{2}\dot{\eta}_a^2 + \frac{1}{2}\dot{\eta}_f^2 + \frac{1}{2}Q^2(\eta_a^2+\eta_f^2) + \\ (\dot{\boldsymbol{r}}_0 \times \boldsymbol{\omega})\cdot(\lambda_a\eta_a + \lambda_f\eta_f)\boldsymbol{e}_3 + \dot{\boldsymbol{r}}_0\cdot(\lambda_a\dot{\eta}_a + \lambda_f\dot{\eta}_f)\boldsymbol{e}_3 + Q^2(\sigma_f\eta_f + \sigma_a\eta_a) - Q(\psi_f\dot{\eta}_f + \psi_a\dot{\eta}_a) \end{aligned} \tag{103}$$

Making the substitution for $\dot{\boldsymbol{r}}_0$, noting that $\dot{\boldsymbol{r}}_0 \times \boldsymbol{\omega} = -Q(\dot{z}-Qx)\boldsymbol{e}_1 + Q(\dot{x}+Qz)\boldsymbol{e}_3$, and using the assumption that $w \approx 0 \Rightarrow \sigma \approx 0$ simplifies the kinetic energy to:

$$\begin{aligned} T = \frac{1}{2}m\Big[(\dot{x}+Qz)^2+(\dot{z}-Qx)^2)\Big] + \frac{1}{2}I_{yy}Q^2 + \frac{1}{2}\dot{\eta}_a^2 + \frac{1}{2}\dot{\eta}_f^2 + \frac{1}{2}Q^2(\eta_a^2+\eta_f^2) + \\ Q(\dot{x}+Qz)(\lambda_a\eta_a + \lambda_f\eta_f) + (\dot{z}-Qx)(\lambda_a\dot{\eta}_a + \lambda_f\dot{\eta}_f) - Q(\psi_f\dot{\eta}_f + \psi_a\dot{\eta}_a) \end{aligned} \tag{104}$$

To determine the potential energy, we can write the gravity in terms of the body-axes using the rotation matrix R_θ:

$$\boldsymbol{g} = g\boldsymbol{n}_3 \tag{105}$$

$$= g(-\sin\theta\boldsymbol{e}_1 + \cos\theta\boldsymbol{e}_3) \tag{106}$$

The gravitational potential is then

$$V_g = -m\boldsymbol{g}\cdot\boldsymbol{r}_0 \tag{107}$$

$$= -mg(-x\sin\theta + z\cos\theta) \tag{108}$$

For the strain energy, we again are only using the fundamental mode shape. It can be shown that the strain energy is

$$V_s = \frac{1}{2}\Big(\omega_f^2\eta_f^2 + \omega_a^2\eta_a^2\Big) \tag{109}$$

Thus, the total potential is

$$V = -mg(-x\sin\theta + z\cos\theta) + \frac{1}{2}\Big(\omega_f^2\eta_f^2 + \omega_a^2\eta_a^2\Big) \tag{110}$$

The Lagrangian for the flexible aircraft is then

$$\begin{aligned} \mathscr{L} &= T - V \\ &= \frac{1}{2}m\Big[(\dot{x}+Qz)^2+(\dot{z}-Qx)^2)\Big] + \frac{1}{2}I_{yy}Q^2 + \frac{1}{2}\dot{\eta}_a^2 + \frac{1}{2}\dot{\eta}_f^2 + \frac{1}{2}Q^2(\eta_a^2+\eta_f^2) + \\ &Q(\dot{x}+Qz)(\lambda_a\eta_a + \lambda_f\eta_f) + (\dot{z}-Qx)(\lambda_a\dot{\eta}_a + \lambda_f\dot{\eta}_f) - Q(\psi_f\dot{\eta}_f + \psi_a\dot{\eta}_a) + \\ &mg(-x\sin\theta + z\cos\theta) - \frac{1}{2}\Big(\omega_f^2\eta_f^2 + \omega_a^2\eta_a^2\Big) \end{aligned} \tag{111}$$

Before proceeding with Lagrange's equations, the virtual work needs to be determined. It is assumed that the aerodynamic and propulsive forces acting on the aircraft (lift, drag, and thrust) are resolved into their body-axis forces such that the forces acting on the aircraft are F_x in the $\boldsymbol{e}_1$ direction and F_z in the $\boldsymbol{e}_3$ direction. The moment about the origin of the inertial triad is $(M + z\,F_x - xF_x)$. For the elastic modes, the modal forces due to the aerodynamics are given by

$$N_f = \int_f p_f(u,t)\phi_f(u)\,du + \sum_{j=1}^{n}\phi_f(u_j)P_{f,j}(t) \tag{112}$$

$$N_a = \int_a p_a(u,t)\phi_a(u)\,du + \sum_{j=1}^{n}\phi_a(u_j)P_{a,j}(t) \tag{113}$$

where $p_a(u,t)$ and $p_f(u,t)$ are the distributed forces (pressures) on the aft and forward beams respectively. The concentrated forces are given by P_f and P_a. To include the effects of damping, we assume that the damping force is proportional to the modal velocities $\dot{\eta}_f$ and $\dot{\eta}_a$. The damping force is given as $2\zeta\omega\dot{\eta}$. The virtual work given in the body axis frame is then

$$\delta W = F_x\delta x + F_z\delta z + (M + z\,F_x - x\,F_z)\delta\theta + (-2\zeta\omega_f\dot{\eta}_f + N_f)\delta\eta_f + (-2\zeta\omega_a\dot{\eta}_a + N_a)\delta\eta_a \tag{114}$$

The generalized coordinates are x, z, θ, η_f, and η_a. Applying Lagrange's Equations, and using the definitions $U \triangleq \dot{x} + Qz$ and $W \triangleq \dot{z} - Qx$, we obtain the following set of differential equations that completely describe the motion of the flexible vehicle:

$$m\dot{U} + mQW + mg\sin\theta + \dot{Q}(\lambda_a\eta_a + \lambda_f\eta_f) + 2Q(\lambda_a\dot{\eta}_a + \lambda_f\dot{\eta}_f) = F_x \tag{115}$$

$$m\dot{W} - mQU - mg\cos\theta + \lambda_a\ddot{\eta}_a + \lambda_f\ddot{\eta}_f - Q^2(\lambda_a\eta_a + \lambda_f\eta_f) = F_z \tag{116}$$

$$(I_{yy} + \eta_a^2 + \eta_f^2)\dot{Q} + (\dot{U} + QW)(\lambda_a\eta_a + \lambda_f\eta_f) + 2Q(\eta_a\dot{\eta}_a + \eta_f\dot{\eta}_f) - \psi_a\ddot{\eta}_a - \psi_f\ddot{\eta}_f = M \tag{117}$$

$$\ddot{\eta}_f + (\dot{W} - QU)\lambda_f - \dot{Q}\psi_f + 2\zeta\omega_f\dot{\eta}_f + (\omega_f^2 - Q^2)\eta_f = N_f \tag{118}$$

$$\ddot{\eta}_a + (\dot{W} - QU)\lambda_a - \dot{Q}\psi_a + 2\zeta\omega_a\dot{\eta}_a + (\omega_a^2 - Q^2)\eta_a = N_a \tag{119}$$

In addition, we have the kinematic differential equations for the downrange and altitude:

$$\dot{X} = U\cos\theta + W\sin\theta \tag{120}$$

$$\dot{h} = U\sin\theta - W\cos\theta \tag{121}$$

It is interesting to note that the parameters ψ_a, ψ_f, λ_a, and λ_f vanish if the structural model is unconstrained (i.e., a free-free beam). In the case of an unconstrained structure, the flexural mode shapes are orthogonal to the rigid body rotation, hence the integrals that capture the coupling between the rigid body motion and the flexible modes are now zero. This in turn decouples the elastic modes and the rigid body modes and one is left with a set of equations for the traditional rigid body motion $(\dot{U}, \dot{W}, \dot{Q})$, and a set for the flexible modes. Because we have chosen a constrained beam to model the aircraft flexible modes, we must carry along extra terms to account for the coupling. In addition, if one assumes an infinitely rigid structure such that $\eta_f = \eta_a = 0$, we recover the body axis equations-of-motion for a rigid aircraft.

Stability Axis Equations-of-Motion

Since the aerodynamic forces are written in terms of the lift and drag acting on the vehicle, it is advantageous to re-write the body-axis equations of motion in terms of the stability axes. The transformation matrix $\mathcal{R}_\alpha$, defined in the previous section, that carries the body axes to the stability axes and the following definitions: $\tan\alpha \triangleq W/U$, $V_T^2 \triangleq U^2 + W^2$, $\dot{V}_T = (U\dot{U} + W\dot{W})/V_T$, and $\dot{\alpha} = (U\dot{W} - W\dot{U})/(U^2 + W^2)$ are used to obtain the stability axis equations-of-motion. The stability axis equations-of-motion are omitted for brevity, but are easily obtained using any available software package that performs symbolic mathematics.

Modal Analysis

The vehicle was trimmed at Mach 8 and altitude of 85,000 ft, then subsequently linearized about this trim condition. The open-loop poles of the linearized dynamics are given in Table 1. Note that the aircraft has an unstable short period mode and an unstable phugoid mode. The time to double for the phugoid mode is approximately 3600 sec. The altitude mode is stable, although it is a very slow mode. The structural modes are comprised of two stable complex-conjugate pairs. Note the presence of a pair of high frequency complex-conjugate poles. These two poles are attributed to the aeroelastic mode of the aircraft. The second set of complex-conjugate poles are associated with the bending mode frequency of the fuselage (18 rad/sec) since this is very close to the natural frequency of its first bending mode. Analysis of the eigenvectors tells us that the most significant contributions are due to $\dot{\eta}_a$ followed by $\dot{\eta}_f$ for the first eigenvalue in Table 1. For the second eigenvalue, the eigenvector is dominated by $\dot{\eta}_f$ then $\dot{\eta}_a$. The eigenvectors for the short period mode exhibit the expected contributions from α and Q, but there are even larger contributions from both

Eigenvalue	Damping Ratio	Natural Freq. (rad/s)	Mode
$-2.70 \pm 45.2j$	0.0597	45.3	Aeroelastic
$-0.376 \pm 16.2j$	0.0231	16.2	Flex
-1.95	1.00	1.95	Short Period
1.85	-1.00	1.85	Short Period
-1.45×10^{-3}	1.00	1.45×10^{-3}	Altitude
$1.90 \times 10^{-4} \pm 0.0294j$	-6.44×10^{-3}	0.0294	Phugoid

Table 1. Eigenvalues of Linearized System

State	Aeroelastic	Flex	Short Period	Short Period
V_t	$0.0020 \mp 0.0000j$	$-0.0006 \pm 0.0000j$	0.1480	0.1472
α	$0.0000 \pm 0.0000j$	$-0.0000 \mp 0.0000j$	-0.0034	0.0038
Q	$-0.0008 \mp 0.0000j$	$0.0000 \mp 0.0000j$	-0.0049	-0.0052
h	$0.0001 \pm 0.0011j$	$-0.0000 \mp 0.0008j$	-1.0000	1.0000
θ	$0.0000 \pm 0.0000j$	$-0.0000 \mp 0.0000j$	-0.0036	0.0036
η_f	$0.0008 \pm 0.0145j$	$-0.0013 \mp 0.0568j$	-0.1523	0.1697
$\dot{\eta}_f$	$-0.6904 \mp 0.0024j$	$0.9979 \mp 0.0021j$	-0.2099	-0.2461
η_a	$0.0012 \pm 0.0209j$	$0.0003 \pm 0.0266j$	-0.1047	0.1165
$\dot{\eta}_a$	$-0.9983 \pm 0.0017j$	$-0.4668 \mp 0.0051j$	-0.1442	-0.1690

Table 2. Eigenvectors of Linearized System

η's and $\dot{\eta}$'s, highlighting the inertial coupling between normal acceleration, pitch rate, and the aeroelastic modes of the aircraft.

The poles and zeros are shown in Figure 9 for a 2×2 system where the inputs are the elevator deflection, δ_e, and the change in total temperature in the combustor, ΔT_0. The outputs are the aircraft velocity, V_t, and the flight-path angle, $\gamma = \theta - \alpha$. Note that there are two pairs of complex-conjugate transmission zeros that are mirror images about the $j\omega$ axis. These zero pairs are associated with the flexible mode of the aircraft. The two real zeros seen in Figure 9 that are a mirror image about imaginary axis arise because of the flight-path angle dynamics. To command an increase in flight path angle requires that the elevator deflect trailing edge up to create a nose-up pitching moment. Deflecting the elevator trailing edge up will reduce the lift on the tail, causing an initial drop in the flight-path angle and the altitude. The impact of this low frequency right-half plane transmission zero is that it will severely restrict the bandwidth of the flight control system.

Conclusions

A comprehensive, non-linear model of the aerodynamics, propulsion, and structural dynamics for a representative air-breathing hypersonic vehicle has been presented. The model was derived from first principles and captures the interaction between the propulsion system, the aerodynamics, and the structural dynamics. The equations-of-motion for the flexible aircraft were derived using Lagrange's Equations and include the effects of pitch acceleration and normal acceleration on the structural modes. The linearized aircraft model has unstable short period and phugoid modes, and exhibits a high degree of coupling between the short period and the first bending mode of the fuselage. We also showed that the aircraft model indicates that the flight control system performance is limited due to the presence of a low-frequency right-half plane transmission zero.

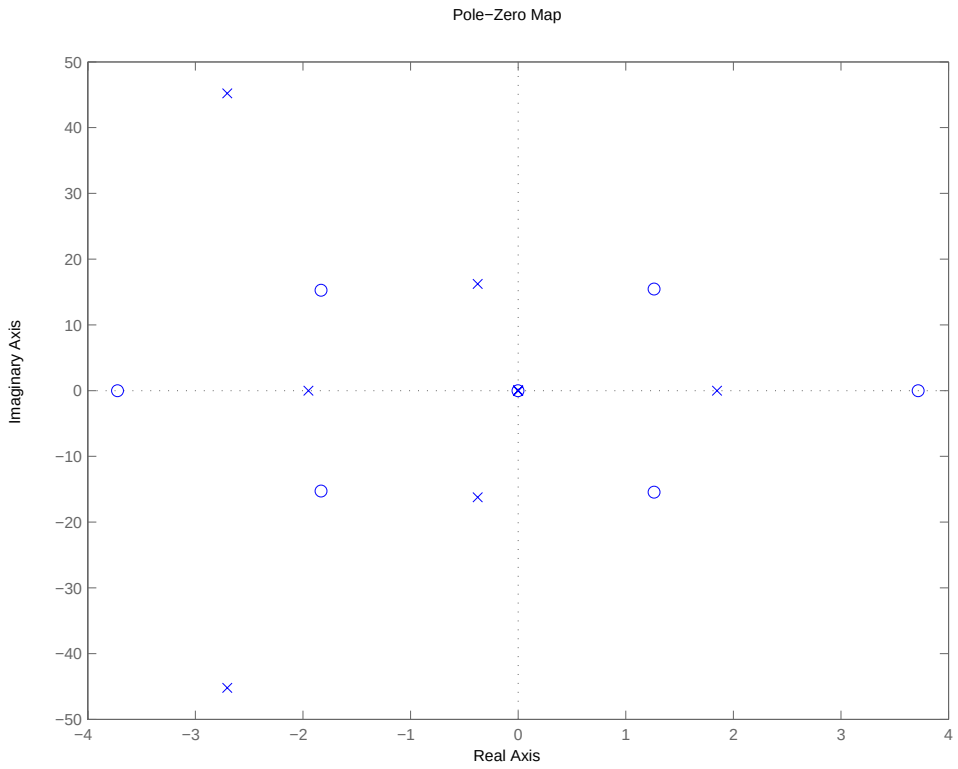

Figure 9. Poles and Transmission Zeros of the Linearized System

Acknowledgements

This work was performed while the first author held a National Research Council Research Associateship Award at the Air Force Research Laboratory.

References

[1]Schmidt, D., "Dynamics and Control of Hypersonic Aeropropulsive/Aeroelastic Vehicles," August 1992, AIAA Paper AIAA-92-4326.

[2]McRuer, D., "Design and Modeling Issues for Integrated Airframe/Propulsion Control of Hypersonic Flight Vehicles," *Proceedings of the 1992 American Control Conference, Boston, MA, June, 1991*, pp. 729–34.

[3]Chavez, F. and Schmidt, D., "Analytical Aeropropulsive/Aeroelastic Hypersonic-Vehicle Model with Dynamic Analysis," *Journal of Guidance, Control, and Dynamics*, Vol. 17, No. 6, Nov-Dec 1994, pp. 1308– 1319.

[4]Schmidt, D. and Velapoldi, J., "Flight Dynamics and Feedback Guidance Issues for Hypersonic Airbreathing Vehicles," *Proceedings of the 1999 Guidance, Navigation, and Control Conference, Portland, OR, Aug. 9-11 1999*, August 1999, AIAA 1999-4122.

[5]von Eggers Rudd, L. and Pines, D., "Integrated Propulsion Effects on the Dynamic Stability and Control of Hypersonic Waveriders," July 2000, AIAA 2000-3826.

[6]"Equations, Tables, and Charts for Compressible Flow," Tech. Rep. NACA-1135, National Advisory Committee for Aeronautics, Ames Aeronautical Laboratory, Moffett Field, CA, 1953.

[7]John, J., *Gas Dynamics*, chap. 10, Allyn and Bacon, 7 Wells Ave, Newton MA 02159, 1984, pp. 139–150.

[8]Bradford, J. and Olds, J., "Improvements and Enhancements to SCCREAM, A Conceptual RBCC Engine Analysis Tool," *AIAA/ASME/SAE/ASEE Joint Propulsion Conference & Exhibit, 34th, Cleveland, OH, July 13-15, 1998*, Paper Number AIAA 98-3775.

[9]Meirovitch, L., *Analytical Methods in Vibrations*, MacMillan Press, 866 Third Ave, New York, N.Y., 1967, pp. 135–143,161–163.

[10]Meirovitch, L., *Analytical Methods in Vibrations*, MacMillan Press, 866 Third Ave, New York, N.Y., 1967, pp. 287–289.

[11]Waszak, M. and Schmidt, D., "Flight Dynamics of Aeroelastic Vehicles," *Journal of Aircraft*, Vol. 25, No. 6, June 1988, pp. 563–571.

[12]Olsen, J., "Unifed Flight Mechanics and Aeroelasticity for Accelerating, Maneuvering, Flexible Aircraft," *RTO AVT Specialists Meeting on "Structural Aspects of Flexible Aircraft Control", Ottawa, CA*, 18-20 October 1999.

[13]Buttrill, C., Zeiler, T., and Arbuckle, P., "Nonlinear Simulation of a Flexible Aircraft in Maneuvering Flight," *AIAA Flight Simulation Technologies Conference, Monterey, CA*, August 17-19 1987, pp. 122–133, AIAA 87-2501.

[14]Meirovitch, L. and Tuzcu, I., "Integrated Approach to the Dynamics and Control of Flexible Manuevering Aircraft," Tech. rep., 2003.